ACS Photonics

Article

pubs.acs.org/journal/apchd5

Third-Order Optical Nonlinearities in Organometallic Methylammonium Lead Iodide Perovskite Thin Films

Basanth S. Kalanoor, Laxman Gouda, Ronen Gottesman, Shay Tirosh, Eynav Haltzi, Arie Zaban, and Yaakov R. Tischler*

Department of Chemistry and Bar-Ilan Institute of Nanotechnology and Advanced Materials, Bar-Ilan University, Ramat Gan, 52900, Israel

Supporting Information

ABSTRACT: With solar conversion efficiencies surpassing 20%, organometallic perovskites show tremendous promise for solar cell technology. Their high brightness has also led to demonstrations of lasing and power-efficient electroluminescence. Here we show that thin films of methylammonium lead iodide, prepared by solution processing at temperatures not exceeding 100 °C, exhibit a highly nonlinear intensity-dependent refractive index due to changes in the free-carrier concentration and for femtosecond excitation at higher intensities undergo saturation that can be attributed to the Pauli blocking effect. Nonlinear refractive index and nonlinear absorption coefficients were obtained by the *Z*-scan technique, performed simultaneously in open- and closed-aperture configurations. Both nanosecond- and femtosecond-pulsed lasers at multiple wavelengths were used in order to distinguish between the mechanisms inducing the nonlinearities. The magnitude and sign of the nonlinear refractive index n_2 were determined. For resonant excitation, free carrier generation is the dominant contribution to the nonlinear refractive index, with a large nonlinear refractive index of $n_2 = 69 \times 10^{-12}$ cm^2/W being observed for resonant femtosecond pumping and $n_2 = 34.4 \times 10^{-9}$ cm^2/W for resonant nanosecond pumping. For nonresonant femtosecond excitation, bound-charge-induced nonlinearity leads to $n_2 = 36 \times 10^{-12}$ cm^2/W. These values are equivalent to the best reported metrics for conventional semiconductors, suggesting that organometallic perovskites are promising materials for optical switching and bistability applications.

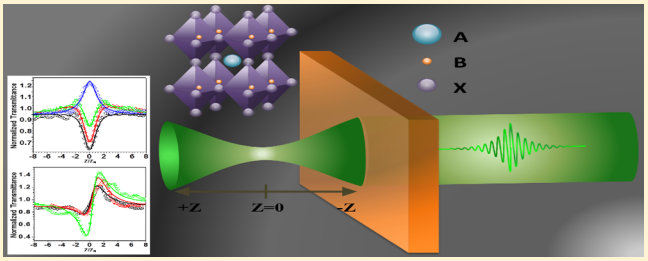

KEYWORDS: *nonlinear optics, Z-scan, organometallic perovskite, Kerr effect, nonlinear refraction, methyl ammonium lead iodide*

Materials exhibiting optical nonlinearities are important elements for applications in optical data storage, optical switches,[1,2] semiconductor optical amplifiers,[3] and lasers.[4] Currently, optical signal switching in optical communications is accomplished through optical-to-electronic-to-optical (OEO) conversion components. All-optical networking can be a solution for providing the huge bandwidth required for future data and communication networks. Therefore, all-optical switches can play an important role in communication speed and capacity. The main physical process governing operation of such a photonic device is photoinduced changes in the refractive index.[5] These changes can be due to the instantaneous Kerr effect, which occurs when bound electronic charges of the material are virtually excited by photons with energies that are below the band gap. The most frequently used nonlinear refractive index material is SiO_2 in the form of optical fibers. Although the effect is weak, long interaction lengths through the fiber ensure appreciable modulation.[6] In thin films, the Kerr effect is generally weak. Excitation of electrons through direct single-photon or multiphoton absorption processes can bring about a change in the refractive index that is considerably larger than the Kerr effect. The carrier-induced refractive index change is polarization and wavelength independent, making it potentially more useful for optical switch applications. However, the response from carrier-induced third-order nonlinearities depends upon the rates of carrier diffusion and recombination. In addition, temperature-induced changes in the refractive index occur simultaneously via changes in the band gap with lattice temperature.

Organometallic perovskites are hybrid semiconductor materials composed of two nested inorganic cages that are ionically bonded to one another with an organic molecule situated in the center.[7] Research on organic−inorganic perovskites originally began two decades ago for possible use in thin film electronics. The goal was to develop semiconductor materials that could be fabricated into thin films via facile, low-temperature, nonvacuum, solution processing and simultaneously provide high-quality device characteristics. While traditional perovskites are typically composed of two different metals and three oxygen atoms per unit cell, organometallic perovskites enable integration of useful organic and inorganic features within a single molecular-scale composite material. Photovoltaic research on methylammonium lead trihalide perovskite absorbers

Received: December 28, 2015
Published: February 2, 2016

DOI: 10.1021/acsphotonics.5b00746
ACS Photonics 2016, 3, 361−370

($CH_3NH_3PbX_3$ or $MAPbX_3$ where X = Br, Cl, I) has led to solar cells with reported certified efficiencies exceeding 20%.[8−10] The $MAPbX_3$ structures possess high optical absorption, a wavelength-tunable band gap that can be optimized for single-cell or tandem-cell applications, and long diffusion lengths for both electrons and holes.[11,12] More recently, $MAPbX_3$ materials were shown to be suitable for other photonic and optoelectronic device applications such as light-emitting diodes, photodetectors, and lasers, which leverage their high photoluminescence efficiency and good electrical transport properties.[13−15]

In light of these developments, we investigated the nonlinear optical properties of organometallic perovskites as a potentially important semiconductor material for all-optical switching. We focused exclusively on the third-order optical nonlinearities in methylammonium lead iodide ($MAPbI_3$) thin films. We characterized the change in refractive index of the material as a function of light intensity, according to the equation $n(I) = n_0 + n_2I$[16] and determined the second-order refraction and nonlinear absorption coefficients at both resonant and nonresonant excitation wavelengths. Third-order nonlinearities of this form are general and apply to nearly all optical materials, as they do not require a specific inversion symmetry of the material unlike in the case of second-order nonlinearities.[16] Hence, their characterization is a natural starting point for understanding the optical nonlinearities of organometallic perovskites.

Understanding the sources for third-order optical nonlinearity is important for developing photonic materials and devices. The sources for the third-order nonlinearities and the consequent refractive index changes can be an instantaneous Kerr effect or charge carrier related.[17] Hence, at the materials level, these measurements are important for ascertaining carrier dynamics, charge trapping, and structural changes. For devices, a large carrier-induced refractive index change would suggest organometallic perovskites can have significant consequences for optical switching and lasing applications, both based on optical pumping and eventual electrical excitation or modulation. A large instantaneous Kerr effect would suggest organometallic perovskites could be useful for ultrafast optical switch applications.[18]

It appears to be an open question as to whether or under what conditions organometallic perovskites are or can be rendered ferroelectric. Researchers have postulated a ferroelectric nature, which plays a critical role in photovoltaic device characteristics and performance.[19,20] On the one hand, ferroelectric effects can explain the undesirable hysteresis in $MAPbX_3$ photovoltaic devices, as the changes occur in the ferroelectric domains and hence built-in potentials that photogenerated charges experience. On the other hand, a ferroelectric character can contribute to higher solar conversion efficiencies due to bulk-photovoltaic effects and quantum coherent wave propagation of excitons that lead to more efficient charge extraction.[20] Indeed, if organometallic perovskites are ferroelectric, one would expect in analogy to other ferroelectric optical materials such as lithium niobate and lead titanate[21−23] that they would be highly nonlinear optical materials. As in other ferroelectrics, the optical nonlinearities would depend on the structural confirmation of the material. One would also anticipate other nonlinear effects to be manifest such as the Pockels effect and second-order nonlinearities, as is the case for lithium niobate, lead titanate, and other such materials, but investigation of these other effects is beyond the scope of the present study.

In this paper, the main aim is to investigate the sources of change in absorption coefficient and refractive index in methylammonium lead iodide perovskite thin films as a function of light intensity. In this direction, both the instantaneous Kerr effect and carrier-induced nonlinearities are characterized, using the *Z*-scan technique with multiple wavelengths and pulse durations for the optical excitation of the perovskite samples. Methylammonium lead iodide perovskite is shown to be a highly nonlinear optical material, possessing strong third-order nonlinearity. To the best of our knowledge, until now there have been no such reports, experimental or theoretical, on $MAPbI_3$.

EXPERIMENTAL DETAILS

Synthesis. For the preparation of $MAPbI_3$ perovskite films, PbI_2 and CH_3NH_3I were used as precursors. The CH_3NH_3I was synthesized using a procedure described elsewhere,[24] while commercial PbI_2 (99.99%, Sigma-Aldrich) was used without further purification. The entire synthesis was performed inside a glovebox. The substrates were 25 × 25 mm microscopic glass slides cleaned using solvents and oxygen plasma cleaning. For the lead iodide precursor, a 1 M solution of PbI_2 in dimethyl sulfoxide (DMSO) was prepared and stirred overnight at 80 °C. Prior to use, the solution was filtered with a PTFE filter that had a pore diameter of 0.45 μm. For the CH_3NH_3I precursor, a solution with a concentration of 32 mg/mL in 2-propanol was prepared immediately before the synthesis and kept at 60 °C. First, a film of PbI_2 was formed on the substrate via spin coating 100 μL of the PbI_2 solution at 4000 rpm for 60 s and then annealed at 100 °C for 60 min. Subsequently, the annealed sample was dipped in the CH_3NH_3I solution for 5 min. Immediately after the dipping, a dark brown color appeared, indicating the formation of the $CH_3NH_3PbI_3$ perovskite. After dipping in the CH_3NH_3I solution, the substrate and perovskite layer were washed with clean 2-propanol. Finally, toluene was spin coated onto the perovskite film at 4000 rpm for 30 s followed by annealing at 100 °C for 45 min. To ensure photostability of the films, samples were packaged following the method described in the SI. To properly characterize packaged samples, we performed *Z*-scan measurements on "empty packages" using all excitation wavelengths and found no nonlinear effects at the intensities used.

Instrumentation. For nonlinear studies, we used a nanosecond Q-switched Nd:YVO_4 laser (Spectra Physics Explorer), operating at a wavelength of 532 nm with a pulse duration of τ_{pulse} = 40 ns in TEM_{00} operation mode. The repetition frequency was fixed at 1 kHz. For femtosecond measurements, the laser source consisted of a Yb:KGW amplifier (Light Conversion Pharos), delivering 200 fs laser pulses, centered at the wavelength of 1028 nm. The repetition rate of the laser was 1 kHz. In order to conduct femtosecond experiments at lower repetition rates, in particular at 500 and 250 Hz, in order to discern thermal contributions, a chopper was inserted in the beam path (Thorlabs MC2000). Femtosecond pulses at 514 nm were obtained by generating the second harmonic of 1028 nm using a BBO nonlinear crystal and filtering out the fundamental with harmonic separators. The *Z*-scan technique and the analysis of the *Z*-scan traces are based on the assumption that the excitation source has a Gaussian beam profile. Hence, before generating *Z*-scan measurements, we characterized the beam quality of each excitation using a beam profiler (Spiricon SP-503U) and confirmed that indeed the beam profile is more than adequately Gaussian. (See the SI for the beam profiles of each excitation.) The transmitted laser beam was divided by means of a beam splitter, providing the two different experimental

DOI: 10.1021/acsphotonics.5b00746
ACS Photonics 2016, 3, 361−370

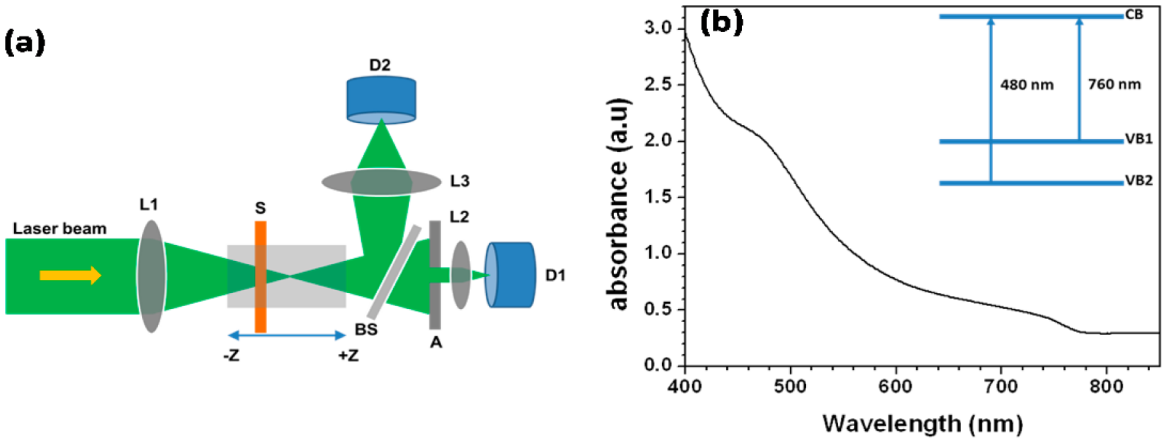

Figure 1. Experimental *Z*-scan setup: L1, L2, and L3, lenses; BS, beam splitter; S, sample; D1 and D2, photodetectors; A, aperture. (b) Ground-state absorption spectra of $CH_3NH_3PbI_3$ with inset showing band structure with dual valence band (VB); (CB) conduction band.

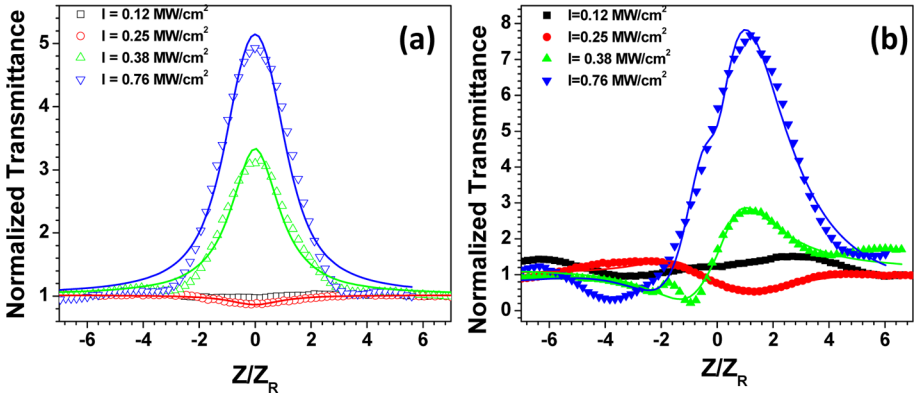

Figure 2. (a) Open-aperture and (b) closed-aperture *Z*-scan traces at different pumping intensities with nanosecond λ = 532 nm laser excitation. Solid lines indicate the theoretical fitting to the measured data.

Table 1. Summary of the Third-Order Nonlinear Optical Parameters Measured at 532 nm with Different Pumping Intensities, All at a Repetition Rate of 1 kHz

wavelength (nm)	pulse width (s)	intensity (MW/cm^2)	saturation intensity (W/cm^2)	β_{eff} (cm/MW)	$n_2 \times 10^{-9}$ (cm^2/W)
532 nm	40 ns	0.25	0.8 ± 0.02	22.2 ± 0.3	−0.41 ± 0.2
		0.38	0.7 ± 0.01	−1620 ± 23	34.4 ± 1.5
		0.76	0.9 ± 0.02	−260 ± 12	10 ± 0.8

configurations (Figure 1a). In open-aperture *Z*-scan, the beam is totally collected by a large-diameter lens, allowing the determination of the nonlinear absorption coefficient. In closed-aperture *Z*-scan, the beam is collected after it passes through a small-diameter iris of 1 mm, placed in the far field to obtain the nonlinear refractive index. The transmitted intensity of each pulse is measured by using a fast response integrating photodetector (Becker and Hickle PDI-400) and sample and hold modules (Becker and Hickle SHM-180). The sample thickness (∼500 nm) was less than the Rayleigh range to fulfill the thin sample approximation condition. In addition, measurements on the 1 mm thick glass substrates and "empty" packages at different laser peak intensities (I_0) were carried out. Measurements of the glass substrates and packaging by themselves did not show a nonlinear response for the intensity ranges that were investigated here and, therefore, confirm that the observed nonlinear behavior is from the properties of the perovskite thin film. We also confirmed that the excitation intensities utilized did not burn the film, by imaging the film before and after laser excitation, as reported in the SI.

Nonlinear Optical Measurements. Measurements of third-order optical nonlinearities were obtained using the *Z*-scan technique. The *Z*-scan is a single excitation beam technique to measure the nonlinear refractive index (NLR) and nonlinear absorption coefficient (NLA) of the materials.[25] The technique provides sensitive and straightforward determination of the sign and the values of the nonlinear refractive index (n_2), the two-photon absorption (TPA) coefficient (β), and the free carrier absorption coefficient (σ). In the *Z*-scan, the variation in the transmission of the excitation laser is measured in the far field as the sample is moved along the direction of propagation through the focus of the beam. The sample experiences a different intensity as it is scanned through the focus, and hence it exhibits a different nonlinear response as a function of position. The presence or absence of an aperture placed in front of a photodetector gives rise to the closed-aperture (CA) and open-aperture (OA) *Z*-scan configurations, respectively. CA *Z*-scan profiles contain contributions from both the NLR and NLA.

Third-order optical nonlinear processes can be divided broadly into two categories: resonant and nonresonant. The resonant

DOI: 10.1021/acsphotonics.5b00746
ACS Photonics 2016, 3, 361−370

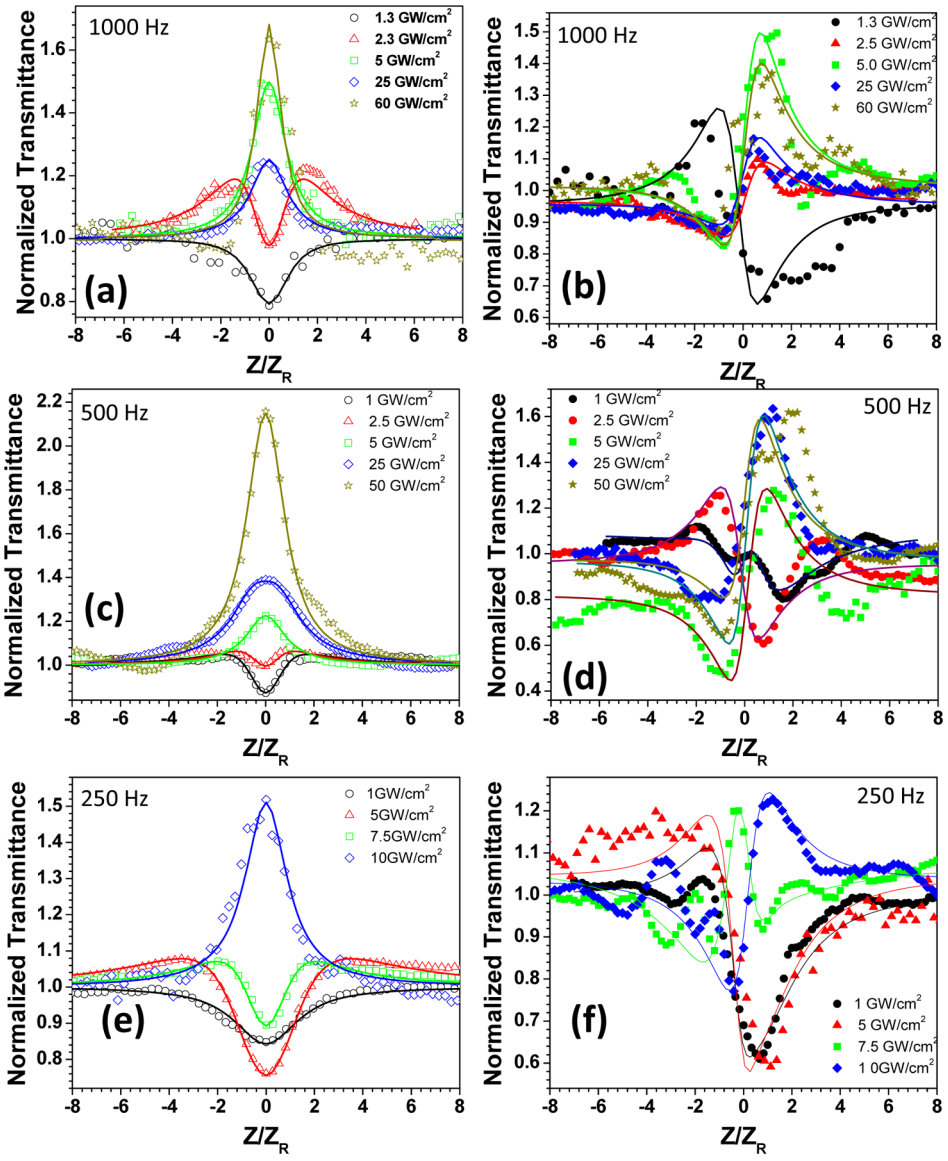

Figure 3. Open-aperture (a) 1000 Hz, (c) 500 Hz, and (e) 250 Hz and closed-aperture (b) 1000 Hz, (d) 500 Hz, and (f) 250 Hz *Z*-scan traces at different pumping intensities with femtosecond laser excitation at a wavelength of 514 nm. Solid lines indicate the theoretical fitting to the measured data.

nonlinearity can arise from the actual transitions and are slow, whereas nonresonant transitions are from virtual transitions and are fast. The change in the nonlinear refractive index can be due to free charge carrier nonlinearity, bound electronic charge nonlinearity, or temperature-induced lensing effects. The details of the measurement determine the contributions from the various possesses.

Free carriers can change the refractive index because of their ability to absorb incident light,[26] and they are generated by a combination of linear and nonlinear optical absorption processes. In the resonant region, the dominant generation mechanism is linear absorption, while in the nonresonant region, it is multiphoton processes. Due to the ease of generating free carriers in semiconductors, large free carrier nonlinearity is possible. For longer excitation pulses, such as in the nanosecond regime, free carriers are the primary contributors to the observed optical nonlinearity, and they can mask the faster responses from bound electronic charge nonlinearity. This is to be contrasted with femtosecond-pulsed excitation, where at low excitation intensity the dominant contribution to the nonlinearity is from the bound charge carriers. With higher pulse intensity, even with subpicosecond pulse durations, the nonlinearity from the free carriers dominates the other processes, as free charges accumulate during the pulse.[27] Under the condition of free carrier absorption, the nonlinear refractive index change (Δn) is given by

$$\Delta n = \gamma I + \sigma N \tag{1}$$

where N is the carrier density generated by the combination of linear and nonlinear absorption and γ is the nonlinear refractive index coefficient due to bound charges.

The measured normalized transmission (T) for CA experiments is given by the expression[28]

$$T(x, s \approx 0) = 1 + \frac{1}{\sqrt{2}}\frac{4x\varphi_0 - (x^2+3)q_0}{(x^2+1)(x^2+9)} + \frac{1}{\sqrt{3}} \times \frac{4\varphi_0^2(3x^2-5) + q_0^2(x^4+17x^2+40) - 8\varphi_0 q_0 x(x^2+9)}{(x^2+1)^2(x^2+9)(x^2+25)} \tag{2}$$

DOI: 10.1021/acsphotonics.5b00746
ACS Photonics 2016, 3, 361−370

where $x = z/z_0$ is the relative sample position, $q_0 = \beta I_0(1 - R) L_{eff}$ is the on-axis phase shift due to the absorptive nonlinearity, $\varphi_0 = 2\pi n_2 I_0(1 - R)L_{eff}/\lambda$ is the on-axis nonlinear refraction phase shift, with $n_2 = \gamma + \sigma N/I$ as the effective nonlinear Kerr index, which is an intensity dependent parameter, $L_{eff} = [1 - \exp(\alpha_0 L)]/\alpha_0$ is the effective sample length, z_0 is the Rayleigh length of the Gaussian beam, I_0 is the on-axis peak intensity of the laser, R is the Fresnel reflectivity coefficient at the interface of the material with air, s is the linear transmittance of the far-field aperture, L is the physical length of the sample, and α_0 is the one-photon absorption coefficient including the contribution from free carrier absorption. The linear absorption coefficient values for our films are 2.5×10^4, 3×10^4, and 6×10^3 cm^{-1} for 532, 514, and 1028 nm, respectively. This equation applies under certain conditions as described elsewhere.[28] In particular, the sample thickness must be less than the Rayleigh range, and the slowly varying envelope approximation must hold, which is consistent with our experimental conditions.

The thermal nonlinear refractive index change is due to the accumulation of thermal effects inside the sample between two acquisition points. The time-dependent expression for normalized transmission for thermal effects is given by[29]

$$T(x, t) = \frac{1}{1 + \left(\frac{\nu}{1 + t_c/2t}\right)\frac{2x}{1 + x^2} + \left(\frac{\nu}{1 + t_c/2t}\right)^2 \frac{x}{1 + x^2}} \quad (3)$$

where t is the elapsed time after the laser pulse traverses the sample, $t_c = \frac{d^2}{4D}$ is the thermal-diffusion time (d is the beam diameter), and D (cm^2 s^{-1}) is the thermal diffusion coefficient of the sample material. The term ν is on the on-axis phase shift and is given by

$$\nu = \frac{\alpha P t}{\lambda \kappa}\frac{dn}{dT} \quad (4)$$

where α is linear absorption coefficient, P is the input pump power, κ is the thermal conductivity of the material, λ is the wavelength of excitation, t is the thickness of the sample, and dn/dT is the thermo-optic coefficient.

The measured OA experimental data are fitted with a model that describes the contributions of two-photon absorption (2PA), saturable absorption (SA) in the nonlinear absorption coefficient, and free carrier absorption as follows:[30]

$$\alpha(I) = \frac{\alpha_0}{1 + I/I_s} + \beta_{eff} I \quad (5)$$

where

$$\beta_{eff} = \beta_0 + \sigma\alpha\tau_0/\hbar\omega \quad (6)$$

where I_s is the saturation intensity for the material to become transparent at the excitation wavelength. ω ($= 2\pi/\lambda$) is the angular frequency, and τ_0 is the pulse width of the laser.

RESULTS AND DISCUSSION

Nanosecond Pumping. Figure 2 shows the Z-scan measurement performed at 532 nm with various pulse energies at a repetition rate of 1 kHz. At a peak power density of 0.12 MW/cm^2, we did not observe a nonlinear effect in the OA measurements (Figure 2a). As the pump power is increased to 0.25 MW/cm^2, a decrease in the normalized transmission is observed in OA. This decrease is indicative of reverse saturable absorption (RSA) due to absorption from free carriers. As the pump intensity is further increased to 0.38 MW/cm^2, an increase in transmission is observed at the focus of the Z-scan due to saturated absorption of the ground state. With further increase in the pump intensity to 0.76 MW/cm^2, the Z-scan followed the same SA behavior profile.

Figure 2b shows the closed-aperture profiles for the same power densities of excitation. At a pump intensity of 0.25 MW/cm^2, a weak "peak−valley" structure is exhibited. This prefocal transmittance maximum (i.e., the peak) followed by a postfocal transmittance minimum (i.e., the valley) is the Z-scan signature of a negative refractive nonlinearity, which results in a self-defocusing effect. With further increase in the pump intensity to 0.38 MW/cm^2, the profile changed to "valley−peak", indicative of positive refractive index nonlinearity. At the same pump intensity of 0.38 MW/cm^2, in OA we observed a shift of profile from RSA to SA, indicating that the change of the refractive index and nonlinear absorption are both attributable to free carrier absorption. With further increase in the pump intensity, the CA Z-scan did not show any appreciable change in profile, consistent with the trend in OA measurements.

The solid lines in Figure 2 show the theoretical fitting to the experimental results using eqs 1−5. The OA profiles are fitted using eq 5 by varying the parameters β_{eff} and I_s. Since several sets of these parameters can fit the data, the appropriate choice was selected based on the criterion that it also fits the CA Z-scan measurements. Indeed, the CA profiles, which are fitted using eqs 2 and 3, depend on the same β_{eff} parameters.

Femtosecond Pumping. Figure 3 shows the Z-scan measurements performed at an excitation wavelength of 514 nm with various energies and at different repetition rates of 1000, 500, and 250 Hz. At low pump intensities the OA measurements show the decrease in the transmittance at the focus, indicating strong absorption. As the pump intensity is increased, we observe a gradual increase in the transmittance at the focus, finally leading to the SA. In the case of CA measurements, the profiles (Figure 3b,d,f) at lower pump intensities show a "peak−valley" structure, which is typical of a self-defocusing third-order nonlinear optical phenomenon. Further

Table 2. Summary of the Third-Order Nonlinear Optical Parameters Measured at 514 nm with Different Pumping Intensities and Repetition Rates

repetition rate (Hz)	intensity (GW/cm^2)	β_{eff} (cm/MW)	$n_2 \times 10^{-12}$ (cm^2/W)
1000	1.3	22 ± 5	48 ± 5
	2.5	15 ± 0.5	10 ± 2
	5	−1.5 ± 0.09	12 ± 3
	25	−0.04 ± 0.002	−0.24 ± 0.08
	60	−0.23 ± 0.02	−0.26 ± 0.07
500	1	34 ± 5	58 ± 7
	2.5	8.9 ± 0.4	26 ± 4
	5	3 ± 0.02	−15 ± 2
	25	0.5 ± 0.02	−2.4 ± 0.5
	50	−0.2 ± 0.02	−1.6 ± 0.2
250	1	18.5 ± 1.5	69 ± 9
	5	4.0 ± 0.08	16 ± 3
	7.5	4.7 ± 0.06	6.1 ± 2
	10	−0.5 ± 0.02	4.9 ± 0.8
	50	−0.20 ± 0.01	−1.30 ± 0.3

DOI: 10.1021/acsphotonics.5b00746
ACS Photonics 2016, 3, 361−370

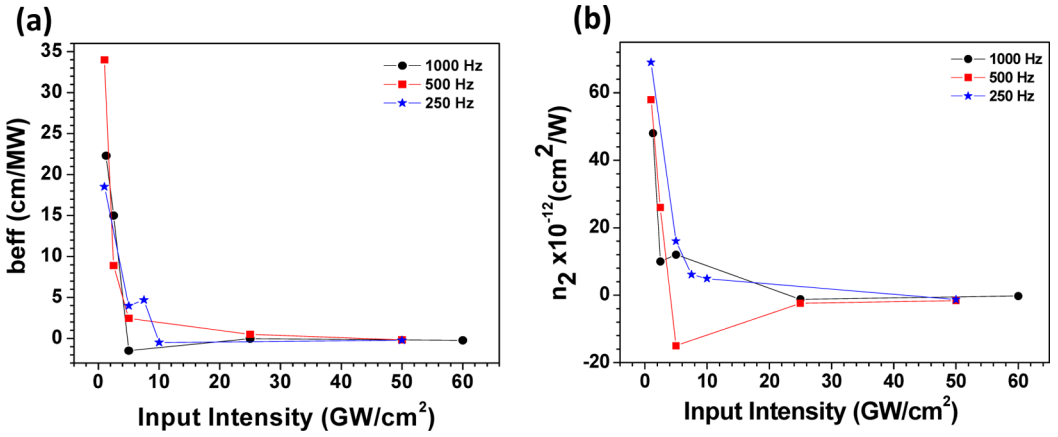

Figure 4. (a) β_{eff} as a function of input intensity; (b) n_2 as a function of input intensity with different repetition rates at 514 nm.

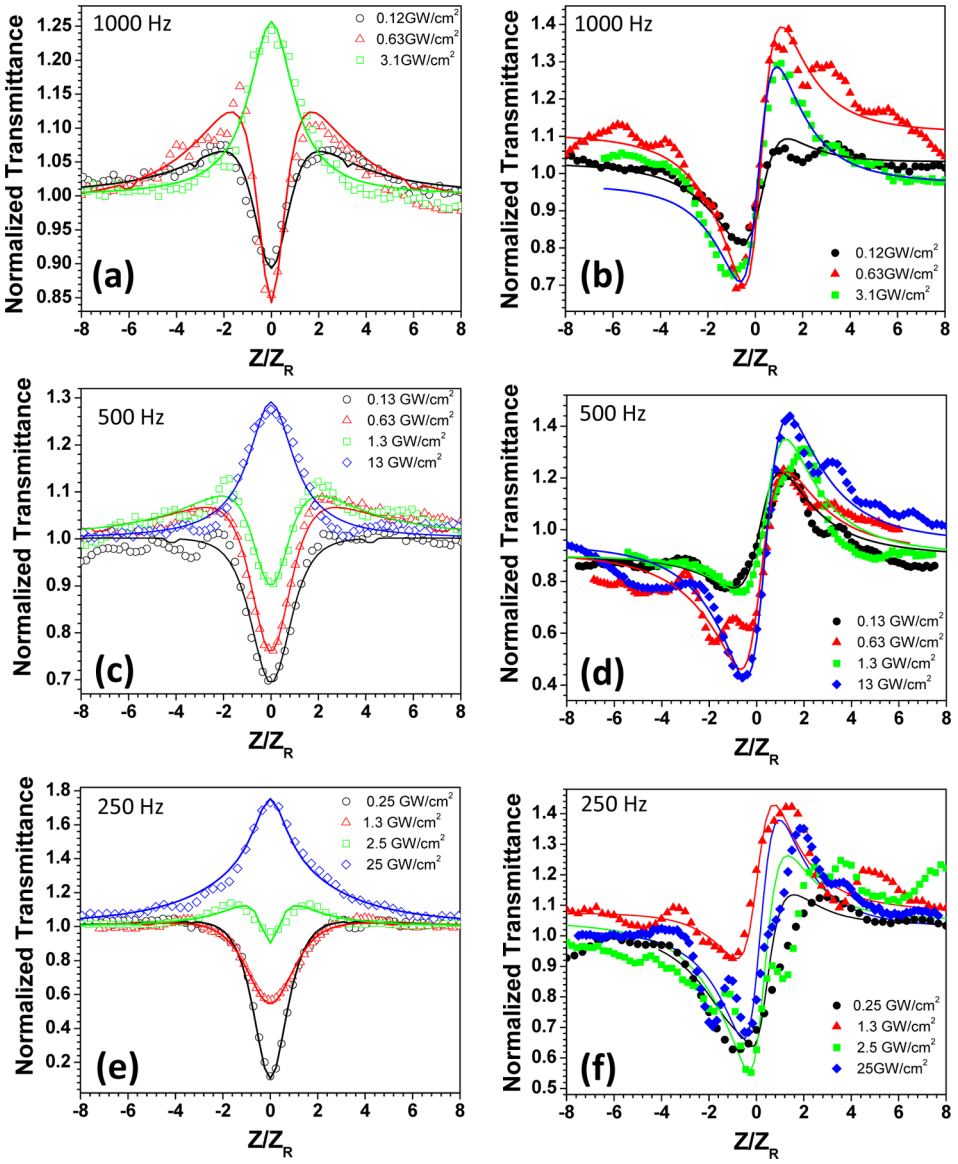

Figure 5. Open-aperture (a) 1000 Hz, (c) 500 Hz, and (e) 250 Hz and closed-aperture (b) 1000 Hz, (d) 500 Hz, and (f) 250 Hz *Z*-scan traces at different pumping intensities with femtosecond laser excitation at a wavelength of 1028 nm. Solid lines indicate the theoretical fitting to the measured data.

increase in the pump intensity showed a change in the nonlinear refractive index in the CA *Z*-scan. This change in the nonlinearity can be attributed to free carrier induced effects, since pump intensity is high enough to generate large carrier concentrations that can thereby induce a change in the refractive index of the material.

DOI: 10.1021/acsphotonics.5b00746
ACS Photonics 2016, 3, 361−370

From the CA traces, as shown in Figure 3, it is apparent that there is greater error in the fits when compared to the open aperture. This higher level of error can be attributed to nonuniformity of the film, which can distort the Gaussian beam profile, thereby inducing artifacts in the closed-aperture profiles.[25] The fit parameters for both open-aperture and closed-aperture traces, for all repetition rates, are summarized in Table 2, and the error bars reflect the relative goodness of the fits.

In order to verify the influence of thermal effects on the *Z*-scan, we performed the measurement at different repetition rates. From Figure 3 we see that there is no change in the profiles at high repetition rate (1000 Hz) compared to that of lower repetition rates (500 Hz, 250 Hz). This confirms that there is no thermal contribution in the femtosecond *Z*-scan measurements.

Figure 4 summarizes the dependence of β_{eff} and n_2 as a function of input intensity and repetition rate. We see that as the pump intensity is increased, the β_{eff} and n_2 decrease and attain saturation at higher intensities. This decrease in the optical nonlinearities is due to their direct dependence on the carrier charge density. Similar decreases of optical nonlinearities are observed in the case of graphene.[31] This indicates that with 514 nm excitation the observed effect is due to the free carrier absorption from direct one-photon optical transition.

To gain a better understanding of the sources of the observed nonlinearities in the $MAPbI_3$ films, additional *Z*-scan measurements were performed using femtosecond excitation at a wavelength of 1028 nm. As the material does not have linear absorption at 1028 nm, any observed nonlinear index change could be attributed to bound electrons or free carriers generated via TPA. Figure 5 shows the CA and OA *Z*-scan measurements performed at 1028 nm.

For OA experiments with 1028 nm excitation, at low intensity we observed a similar decrease in the transmittance at the focus. With a gradual increase in the pump intensity we observed a increase in the transmittance with an increase in the pump intensities. This effect is similar to the one we observed in the case of 514 nm. In the case of CA a valley−peak structure is observed at low pump intensities, indicating positive nonlinear refraction. As the pump intensity is increased, there was no change in the profile as observed in the case of 514 nm.

As shown in Figure 5 the CA traces show a greater error in the fits when compared to the open aperture. This trend is similar to the case of excitation with 514 nm. This higher level of error can be attributed to nonuniformity of the film, as suggested above. The fit parameters for both open-aperture and closed-aperture traces, for all repetition rates, are summarized in Table 3, and the error bars reflect the relative goodness of the fits.

Figure 6 summarizes the dependence of β_{eff} and n_2 as a function of input intensity and repetition rate for 1028 nm excitation. In this case also, we observe similar decreases in β_{eff} and n_2 as the pump intensity is increased, with saturation occurring at higher intensities. This indicates the dependence of the optical nonlinearities on the charge carrier density, when using 1028 nm excitation. Hence, the observed effect can be attributed to changes in free carrier absorption from indirect two-photon optical transition.

Effect of Laser on the Sample. In order to rule out burning effects of the laser excitation on the sample, for each excitation wavelength we repeated the *Z*-scan measurement at the same sample position (Figure 7). As we can see in the *Z*-scan traces, in the regions of the scan that are far from the focus, there is no change in the transmittance, as shown in the OA scans of Figure 7. This indicates that the linear transmission of the perovskite sample was not degraded by the *Z*-scan measurements and confirms that the $MAPbI_3$ film was not damaged by the laser excitation. At the same time, a small change in the measurement is observed between the first *Z*-scan and the second, as the sample is brought through the focus of

Table 3. Summary of the Third-Order Nonlinear Optical Parameters Measured at 1028 nm with Different Pumping Intensities and Repetition Rates

repetition rate (Hz)	intensity (GW/cm^2)	β_{eff} (cm/MW)	$n_2 \times 10^{-12}$ (cm^2/W)
1000	0.1	272 ± 5	19 ± 2
	0.6	17 ± 0.5	13 ± 1
	3.1	−0.5 ± 0.09	2.1 ± 0.2
500	0.1	124 ± 5	36 ± 6
	0.6	23 ± 0.4	14 ± 3
	1.3	7 ± 0.02	4.6 ± 0.3
	13	−0.2 ± 0.02	0.8 ± 0.02
250	0.3	186 ± 2	34 ± 4
	1.3	110 ± 4	4.1 ± 0.2
	2.5	3.6 ± 0.2	3.8 ± 0.09
	25	−0.2 ± 0.05	0.3 ± 0.02

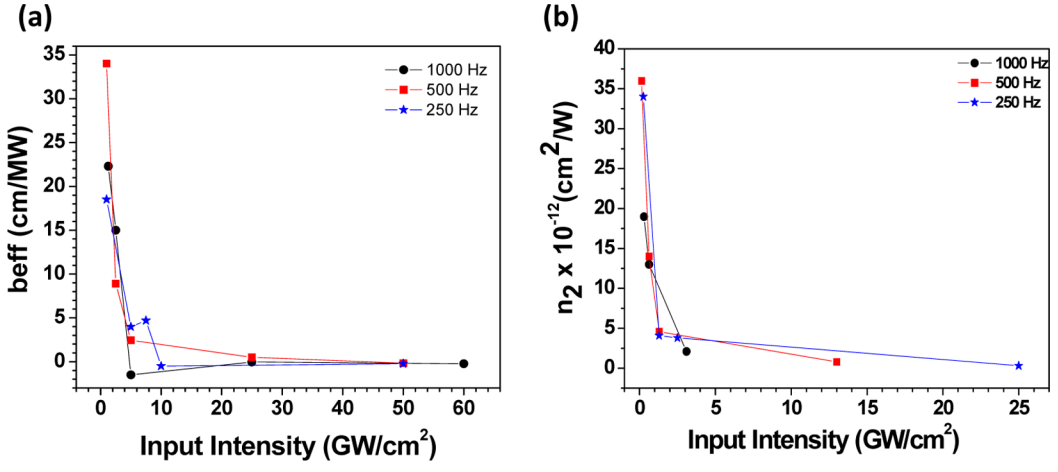

Figure 6. (a) β_{eff} as a function of input intensity; (b) n_2 as a function of input intensity with different repetition rates at 1028 nm.

DOI: 10.1021/acsphotonics.5b00746
ACS Photonics 2016, 3, 361−370

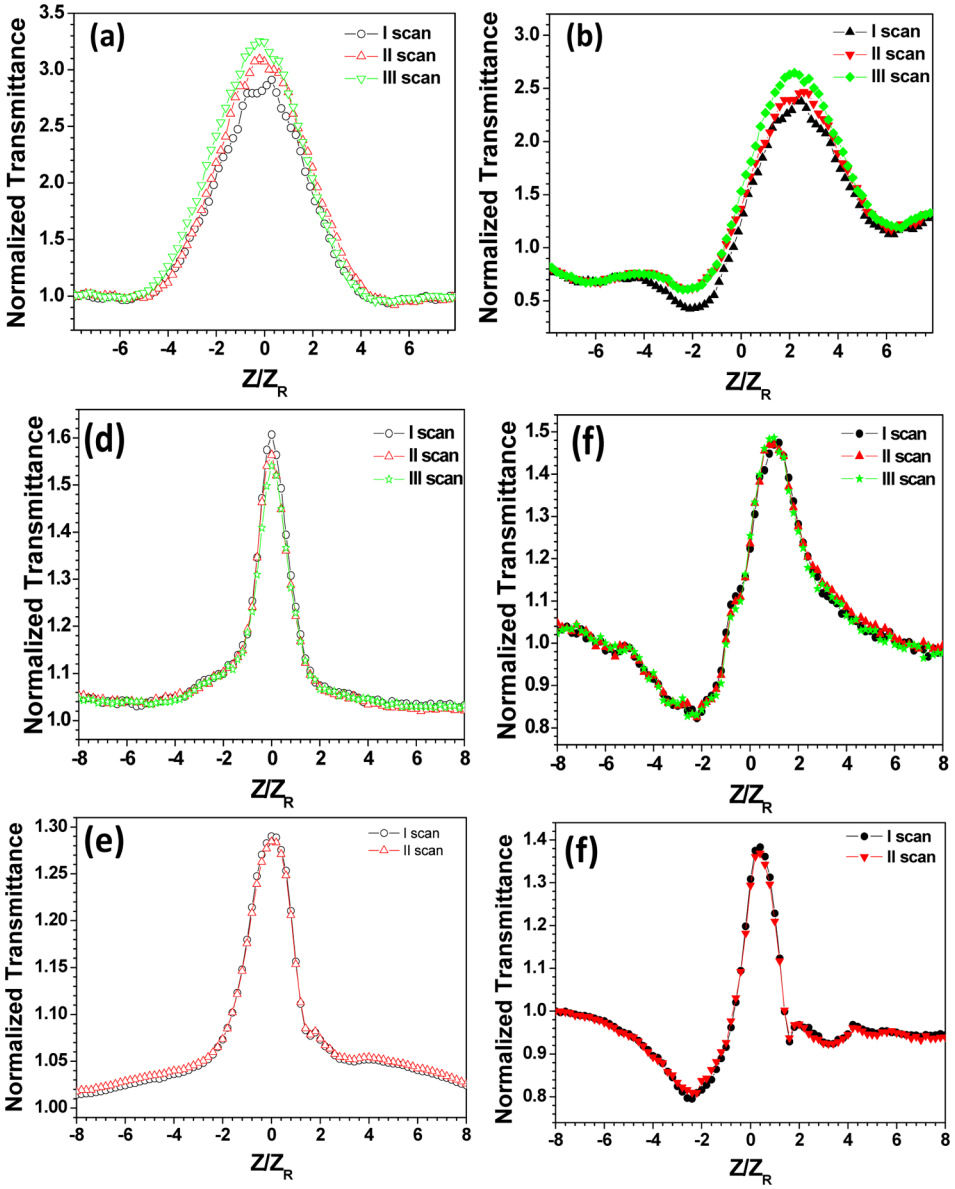

Figure 7. Three sequential *Z*-scans with nanosecond laser excitation of (a) open-aperture and (b) closed-aperture traces at 532, the same position on the sample with the same peak intensity of 0.52 MW/cm^2. Three sequential *Z*-scans with 514 nm femtosecond laser excitation of (c) closed-aperture and (d) open-aperture traces at the same position on the sample with the same peak intensity of 85GW/cm^2. Two sequential *Z*-scans with 1028 nm femtosecond laser excitation of (e) open-aperture and (f) closed-aperture traces at the same position on the sample with the same peak intensity of 50 GW/cm^2. The data show that the linear transmission of the sample was not changed appreciably by the *Z*-scan measurements, confirming that the film was not damaged by the excitation. The solid lines are a guide to the eye.

the laser (Figure 7), suggesting that there may be some re-orientation of molecules within the film.

For CA traces, additional scans at the same position did not show any change in the valley (Figure 7), but a small change after the second scan is observed in the peak of the CA profiles. These changes are most discernible in nanosecond excitation measurements. In addition to the above measurements the observation of the film under microscope did not show any damage from the laser excitation (see the SI for more information). The change in nonlinear refractive index from first to second scans cannot be due to transient thermal effects because the time lapse between subsequent scans is much longer than the thermal relaxation times for the perovskite film. It could be that this change in nonlinear behavior is indicative of a molecular reorganization within the film, which saturates after the second *Z*-scan trace.[24]

The underlying mechanism for observed third-order nonlinear optical behavior can be understood by the energy level diagram as follows. The ground-state absorption spectrum of the perovskite films exhibits two peaks at wavelengths of 480 and 760 nm, as shown in Figure 1b. These peaks arise as a result of the electronic transition from a dual valence band (VB) structure within $MAPbI_3$.[32] Experiments that utilized excitation wavelengths of 532 and 514 nm for nanosecond and femtosecond pumping, respectively, fall in the resonant region of the spectrum. In the resonant region, the laser excitation causes electrons to make a direct transition from VB1 to the conduction band minimum (CB). At a pump intensity of 0.25 MW/cm^2 for ns excitation, a decrease in the transmission is observed, which can be attributed to the initiation of free carrier absorption from VB2 to VB1 and VB1 to CB. As the

DOI: 10.1021/acsphotonics.5b00746
ACS Photonics 2016, 3, 361−370

excitation intensity is further increased, the photogenerated carrier concentration also increases. This leads to the filling of states near the edge of the CB, blocking further absorption via a mechanism know as Pauli blocking.[22] As a result of this band filling, we observe an SA effect in the *Z*-scan profiles in both nanosecond and femtosecond resonant excitation. Working with higher peak intensity showed a strong SA effect because more energy was provided to the system and a higher carrier concentration was generated. For the experiments utilizing a wavelength of 1028 nm, the excitation photon energy lies below the band gap of the VB1 to CB transition and therefore falls in the nonresonant region of the absorption spectrum. Hence, the electrons cannot make a direct transition to the CB via one-photon excitation. The only way the electrons can reach the CB is through TPA. Nevertheless, an SA effect is observed at higher pump intensity in the OA *Z*-scan profiles that again can be attributed to a Pauli blocking effect.

The measured values of the nonlinear refractive index have the same order of magnitude as observed for ferroelectrics such as $Ba_{0.6}Sr_{0.4}TiO_3$ (3.0×10^{-12} cm^2/W), BLFM (2×10^{-12} cm^2/W), and $BiFeO_3$ (1.5×10^{-12} cm^2/W) and for the semiconductors that are typically used in optical switches such as GaAs (3.3×10^{-12} cm^2/W)[33] and Si (3×10^{-12} cm^2/W).[34] Our results suggest that $MAPbX_3$ has significant potential for optical switching applications.

CONCLUSIONS

In this article, the third-order nonlinear optical properties of perovskite $MAPbI_3$ thin films were investigated. The *Z*-scan technique was utilized with a suite of nanosecond and femtosecond pulsed-laser excitations at various wavelengths and repetition rates in order to understand the mechanisms for the nonlinear optical response. For resonant excitation, one-photon-excited interband free carrier absorption is the dominant mechanism responsible for the nonlinearity. In the nonresonant region, bound carriers at lower pump intensities play the dominant role, but at higher pump intensities free carrier and two-photon absorption mechanisms are responsible for the nonlinearity. Ultimately, the nonlinear change in refractive index is achieved through free carrier generation, and for femtosecond excitation at higher intensities it undergoes saturation that can be attributed to a Pauli blocking effect. We have shown that hybrid organometallic semiconductor perovskite $MAPbI_3$ has favorable nonlinear optical properties for eventual use in applications such as optical switching via free carrier injection[35] and also as a depletion mode phase modulator.[36]

ASSOCIATED CONTENT

Supporting Information

The Supporting Information is available free of charge on the ACS Publications website at DOI: 10.1021/acsphotonics.5b00746.

Packaging of the samples to improve photostability, imaging of the perovskite film before and after *Z*-scan measurements to demonstrate their robustness, profiling the excitation beams (PDF)

AUTHOR INFORMATION

Corresponding Author

*E-mail: yrt@biu.ac.il.

Notes

The authors declare no competing financial interest.

ACKNOWLEDGMENTS

We thank the Israel Strategic Alternative Energy Foundation (I-SAEF) and the "Tashtiyot Program" of the Israeli Ministry of Science & Technology for funding this research. A fellowship for L.G. from the European Union Seventh Framework Program Destiny Project, under grant 316494, is acknowledged. We would also like to acknowledge the Israel National Nanotechnology Initiative for providing support through a Focal Technology Area project, FTA grant number 458004.

REFERENCES

(1) Ravindran, S.; Datta, A.; Alameh, K.; Lee, Y. T. GaAs based long-wavelength microring resonator optical switches utilising bias assisted carrier-injection induced refractive index change. *Opt. Express* **2012**, *20*, 15610−15627.

(2) Geldenhuys, R.; van der Merwe, J. S.; Thakulsukanant, K.; Wang, Z.; Chi, N.; Yu, S. Contention resolution and variable length optical packet switching using the active vertical-coupler-based optical Crosspoint switch. *Opt. Switch. Netw* **2011**, *8*, 86−92.

(3) Connelly, M. J. Theoretical calculations of the carrier induced refractive index change in tensile-strained InGaAsP for use in 1550 nm semiconductor optical amplifiers. *Appl. Phys. Lett.* **2008**, *93*, 181111.

(4) Shin, S.; Su, C. B. Strong increase of the derivative of the carrier-induced index change of semiconductor lasers at low injected carrier density. *IEEE Photonics Technol. Lett.* **1993**, *5*, 981−983.

(5) Miller, A.; Welford, K. R.; Daino, B. *Nonlinear Optical Materials and Devices for Applications in Information Technology*; Springer, 1995.

(6) Lin, Q.; Painter, O. J.; Agrawal, G. P. Nonlinear optical phenomena in silicon waveguides: Modeling and applications. *Opt. Express* **2007**, *15*, 16604−16644.

(7) Mitzi, D. B. In *Progress in Inorganic Chemistry*; John Wiley & Sons, Inc., 2007; pp 1−121.

(8) Lee, M. M.; Teuscher, J.; Miyasaka, T.; Murakami, T. N.; Snaith, H. J. Efficient Hybrid Solar Cells Based on Meso-Superstructured Organometal Halide Perovskites. *Science* **2012**, *338*, 643−647.

(9) Burschka, J.; Pellet, N.; Moon, S.-J.; Humphry-Baker, R.; Gao, P.; Nazeeruddin, M. K.; Gratzel, M. Sequential deposition as a route to high-performance perovskite-sensitized solar cells. *Nature* **2013**, *499*, 316−319.

(10) Liu, M.; Johnston, M. B.; Snaith, H. J. Efficient planar heterojunction perovskite solar cells by vapour deposition. *Nature* **2013**, *501*, 395−398.

(11) Xing, G.; Mathews, N.; Sun, S.; Lim, S. S.; Lam, Y. M.; Grätzel, M.; Mhaisalkar, S.; Sum, T. C. Long-Range Balanced Electron- and Hole-Transport Lengths in Organic-Inorganic CH3NH3PbI3. *Science* **2013**, *342*, 344−347.

(12) Stranks, S. D.; Eperon, G. E.; Grancini, G.; Menelaou, C.; Alcocer, M. J. P.; Leijtens, T.; Herz, L. M.; Petrozza, A.; Snaith, H. J. Electron-Hole Diffusion Lengths Exceeding 1 Micrometer in an Organometal Trihalide Perovskite Absorber. *Science* **2013**, *342*, 341−344.

(13) Deschler, F.; Price, M.; Pathak, S.; Klintberg, L. E.; Jarausch, D.-D.; Higler, R.; Hüttner, S.; Leijtens, T.; Stranks, S. D.; Snaith, H. J.; Atatüre, M.; Phillips, R. T.; Friend, R. H. High Photoluminescence Efficiency and Optically Pumped Lasing in Solution-Processed Mixed Halide Perovskite Semiconductors. *J. Phys. Chem. Lett.* **2014**, *5*, 1421−1426.

(14) Sutherland, B. R.; Hoogland, S.; Adachi, M. M.; Wong, C. T. O.; Sargent, E. H. Conformal Organohalide Perovskites Enable Lasing on Spherical Resonators. *ACS Nano* **2014**, *8*, 10947−10952.

(15) Tan, Z.-K.; Moghaddam, R. S.; Lai, M. L.; Docampo, P.; Higler, R.; Deschler, F.; Price, M.; Sadhanala, A.; Pazos, L. M.; Credgington, D.; Hanusch, F.; Bein, T.; Snaith, H. J.; Friend, R. H. Bright light-emitting diodes based on organometal halide perovskite. *Nat. Nanotechnol.* **2014**, *9*, 687−692.

(16) Boyd, R. W. *Nonlinear Optics*; Academic Press, 2003.

DOI: 10.1021/acsphotonics.5b00746
ACS Photonics 2016, 3, 361−370

(17) Sheik-Bahae, M.; Hagan, D. J.; Van Stryland, E. W. Dispersion and band-gap scaling of the electronic Kerr effect in solids associated with two-photon absorption. *Phys. Rev. Lett.* **1990**, *65*, 96−99.
(18) Dakin, J. P.; Brown, R. G. W. *Handbook of Optoelectronics (Two-Vol. Set)*; Taylor & Francis, 2010.
(19) Frost, J. M.; Butler, K. T.; Brivio, F.; Hendon, C. H.; van Schilfgaarde, M.; Walsh, A. Atomistic Origins of High-Performance in Hybrid Halide Perovskite Solar Cells. *Nano Lett.* **2014**, *14*, 2584−2590.
(20) Grinberg, I.; West, D. V.; Torres, M.; Gou, G.; Stein, D. M.; Wu, L.; Chen, G.; Gallo, E. M.; Akbashev, A. R.; Davies, P. K.; Spanier, J. E.; Rappe, A. M. Perovskite oxides for visible-light-absorbing ferroelectric and photovoltaic materials. *Nature* **2013**, *503*, 509−512.
(21) Bing, G.; Hui-Tian, W. Linear and Nonlinear Optical Properties of Ferroelectric Thin Films. In *Ferroelectrics−Physical Effects*; InTech, 2011.
(22) Henari, F. Z.; Cazzini, K.; El Akkari, F.; Blau, W. J. Beam waist changes in lithium niobate during Z-scan measurement. *J. Appl. Phys.* **1995**, *78*, 1373−1375.
(23) Wenjian, L.; Chuanren, Y.; Jihua, Z.; Hongwei, C.; Wencheng, H.; Hong, J.; Jinlong, T.; Wenfeng, Q.; Junjian, L.; Hui, L.; Lifeng, G. Nonlinear Optical Properties of the Lanthanum-Modified Lead Zirconate Titanate Ferroelectric Thin Films Using Z -Scan Technique. *Jpn. J. Appl. Phys., Part 2* **2007**, *46*, L7.
(24) Gottesman, R.; Haltzi, E.; Gouda, L.; Tirosh, S.; Bouhadana, Y.; Zaban, A.; Mosconi, E.; De Angelis, F. Extremely Slow Photoconductivity Response of CH3NH3PbI3 Perovskites Suggesting Structural Changes under Working Conditions. *J. Phys. Chem. Lett.* **2014**, *5*, 2662−2669.
(25) Sheik-Bahae, M.; Said, A. A.; Wei, T. H.; Hagan, D. J.; Van Stryland, E. W. Sensitive measurement of optical nonlinearities using a single beam. *IEEE J. Quantum Electron.* **1990**, *26*, 760−769.
(26) Bulutay, C.; Turgut, C. M.; Zakhleniuk, N. A. Carrier-induced refractive index change and optical absorption in wurtzite InN and GaN: Full-band approach. *Phys. Rev. B: Condens. Matter Mater. Phys.* **2010**, *81*, 155206.
(27) Said, A. A.; Sheik-Bahae, M.; Hagan, D. J.; Wei, T. H.; Wang, J.; Young, J.; Van Stryland, E. W. Determination of bound-electronic and free-carrier nonlinearities in ZnSe, GaAs, CdTe, and ZnTe. *J. Opt. Soc. Am. B* **1992**, *9*, 405−414.
(28) Gu, B.; Ji, W.; Huang, X.-Q. Analytical expression for femtosecond-pulsed Z scans on instantaneous nonlinearity. *Appl. Opt.* **2008**, *47*, 1187−1192.
(29) Cuppo, F. L. S. A.; Figueiredo Neto, A. M.; Gómez, S. L.; Palffy-Muhoray, P. Thermal-lens model compared with the Sheik-Bahae formalism in interpreting Z-scan experiments on lyotropic liquid crystals. *J. Opt. Soc. Am. B* **2002**, *19*, 1342−1348.
(30) Kumar, S.; Anija, M.; Kamaraju, N.; Vasu, K. S.; Subrahmanyam, K. S.; Sood, A. K.; Rao, C. N. R. Femtosecond carrier dynamics and saturable absorption in graphene suspensions. *Appl. Phys. Lett.* **2009**, *95*, 191911.
(31) Bao, Q.; Zhang, H.; Wang, Y.; Ni, Z.; Yan, Y.; Shen, Z. X.; Loh, K. P.; Tang, D. Y. Atomic-Layer Graphene as a Saturable Absorber for Ultrafast Pulsed Lasers. *Adv. Funct. Mater.* **2009**, *19*, 3077−3083.
(32) Stamplecoskie, K. G.; Manser, J. S.; Kamat, P. V. Dual nature of the excited state in organic-inorganic lead halide perovskites. *Energy Environ. Sci.* **2015**, *8*, 208−215.
(33) Hurlbut, W. C.; Lee, Y.-S.; Vodopyanov, K. L.; Kuo, P. S.; Fejer, M. M. Multiphoton absorption and nonlinear refraction of GaAs in the mid-infrared. *Opt. Lett.* **2007**, *32*, 668−670.
(34) Bristow, A. D.; Rotenberg, N.; van Driel, H. M. Two-photon absorption and Kerr coefficients of silicon for 850−2200nm. *Appl. Phys. Lett.* **2007**, *90*, 191104.
(35) Ishida, K.; Nakamura, H.; Matsumura, H.; Kadoi, T.; Inoue, H. InGaAsP/InP optical switches using carrier induced refractive index change. *Appl. Phys. Lett.* **1987**, *50*, 141−142.
(36) Mendoza-Alvarez, J. G.; Yan, R. H.; Coldren, L. A. Contribution of the band-filling effect to the effective refractive-index change in double-heterostructure GaAs/AlGaAs phase modulators. *J. Appl. Phys.* **1987**, *62*, 4548−4553.

DOI: 10.1021/acsphotonics.5b00746
ACS Photonics 2016, 3, 361−370